
Improve Single-Point Zeroth-Order Optimization Using High-Pass and Low-Pass Filters

Xin Chen

School of Engineering and Applied Sciences
Harvard University
chen_xin@g.harvard.edu

Yujie Tang

School of Engineering and Applied Sciences
Harvard University
yujietang@seas.harvard.edu

Na Li

School of Engineering and Applied Sciences
Harvard University
nali@seas.harvard.edu

Abstract

Single-point zeroth-order optimization (SZO) is suitable for solving online black-box optimization and simulation-based learning-to-control problems. However, the vanilla SZO method suffers from larger variance and slow convergence, which seriously limits its practical application. On the other hand, extremum seeking (ES) control is regarded as the continuous-time version of SZO, while they have been mostly studied separately in the control and optimization communities despite the close relation. In this work, we borrow the idea of high-pass and low-pass filters from ES control to improve the performance of SZO. Specifically, we develop a novel SZO method called HLF-SZO, by integrating a high-pass filter and a low-pass filter into the vanilla SZO method. Interestingly, it turns out that the integration of a high-pass filter coincides with the residual-feedback SZO method, and the integration of a low-pass filter can be interpreted as the momentum method. We prove that HLF-SZO achieves a convergence rate of $O(d/T^{\frac{2}{3}})$ for Lipschitz and smooth objective functions (in both convex and nonconvex cases). Extensive numerical experiments show that the high-pass filter can significantly reduce the variance and the low-pass filter can accelerate the convergence. As a result, the proposed HLF-SZO has a much smaller variance and much faster convergence compared with the vanilla SZO method, and empirically outperforms the state-of-the-art residual-feedback SZO method.

1 Introduction

In this paper, we consider solving the generic unconstrained optimization problem:

$$\min_{\mathbf{x} \in \mathbb{R}^d} f(\mathbf{x}), \quad (1)$$

where $\mathbf{x} \in \mathbb{R}^d$ is the decision variable and $f : \mathbb{R}^d \rightarrow \mathbb{R}$ is the objective function. A straightforward solution is to apply the gradient descent methods [1], e.g., $\mathbf{x}_{k+1} = \mathbf{x}_k - \eta \cdot \nabla f(\mathbf{x}_k)$ with the step size η . However, in many practical applications, the first-order information of function f , i.e., the gradient $\nabla f(\mathbf{x})$, may be unavailable or too expensive to procure, and one can only access the zeroth-order information, i.e., function evaluations. To this end, zeroth-order (or derivative-free) methods [2] are developed for black-box optimization, which essentially estimate the gradients using perturbed function evaluations. Zeroth-order optimization (ZO) has attracted a great deal of recent attention and has been used for a broad spectrum of applications, such as reinforcement learning [3, 4], adversarial training [5], power system control [6, 7], online sensor management [8], etc.

According to the number of queried function evaluations at each iteration, ZO methods can be categorized into two types: single-point and multi-point [8]. As suggested by the name, single-point ZO (SZO) [9] only needs to query the function value once at each iteration, making it particularly suitable for online optimization problems. In contrast, multi-point ZO, such as two-point ZO [10], requires two or more function evaluations at each iteration, which may not be applicable to online optimization and decision-making problems in dynamic environments [11]. Nevertheless, it is known that the vanilla SZO method [9] suffers from slow convergence and a large estimation variance [9, 11], which seriously jeopardizes its practical application. Improving the performance of SZO has become an active research topic [11, 12, 13], and the residual-feedback SZO scheme proposed in the recent work [11] achieves the state-of-the-art performance to date.

In the control field, there is a continuous-time version of SZO called *extremum seeking (ES) control* [14, 15]. ES control is a classic adaptive control technique that uses only output feedback to steer a dynamical system to a state where the output attains an extremum. It can also be adopted as a derivative-free algorithm to solve static-map optimization problems [15, 16, 17]. In addition, although not essential for system operation, a *high-pass filter* and a *low-pass filter* are generally integrated into the ES control systems, because these filters can significantly improve transient behavior and mitigate oscillations. See Section 2 for detailed explanations. Despite the close connection between ES control and SZO, these two approaches have been mostly studied separately in the control and optimization communities. Then a natural question to ask is

“Can we borrow some useful tools developed in extremum seeking control, such as the high-pass and low-pass filters, to improve the performance of single-point zeroth-order optimization?”

Motivated by this question, we explore a new path to enhance SZO through leveraging high-pass and low-pass filters from ES control.

Contributions. In this paper, we develop a novel SZO scheme called **HLF-SZO (High/Low-pass Filter Single-point ZO)** by integrating a high-pass filter and a low-pass filter into the vanilla SZO method. We reveal that the integration of a high-pass filter coincides with the residual-feedback SZO scheme proposed in [11], which can significantly reduce the variance; and the integration of a low-pass filter can be interpreted as the momentum (heavy-ball) method [18], which can further accelerate the convergence. Moreover, we prove that HLF-SZO achieves a convergence rate of $O(d/T^{\frac{2}{3}})$ for Lipschitz and smooth objective functions (in both convex and nonconvex cases), which is better than the rate $O(d^2/T^{\frac{2}{3}})$ of residual-feedback SZO given in [11] and inferior to the two-point ZO with a rate of $O(d/T)$ [2]. In addition, extensive numerical experiments demonstrate that the proposed HLF-SZO method exhibits a much smaller variance and much faster convergence compared with the vanilla SZO method, and empirically outperforms the residual-feedback SZO method.

Connecting ES control and ZO to benefit each other is an interesting direction that deserves more research, and our work is a preliminary attempt to throw light on this direction. For example, this work only considers the simplest high-pass and low-pass filters, while higher-order filters or compensators with more complex designs have been used in ES control to enhance stability and transient performance [19], which may be also applicable to ZO methods for further improvement.

Notations. We let $\mathbb{B}_d := \{\mathbf{x} \in \mathbb{R}^d : \|\mathbf{x}\| \leq 1\}$ denote the closed unit ball of dimension d , and let $\mathbb{S}_{d-1} := \{\mathbf{x} \in \mathbb{R}^d : \|\mathbf{x}\| = 1\}$ denote the unit sphere.

2 Preliminaries on ZO and ES Control

2.1 Zeroth-Order Optimization Methods

A popular ZO approach is to estimate the gradient $\nabla f(\mathbf{x})$ with only one function value query. Specifically, upon defining

$$\mathbf{G}_f^{(1)}(\mathbf{x}; r, \mathbf{u}) := \frac{d}{r} f(\mathbf{x} + r\mathbf{u})\mathbf{u}, \quad (2)$$

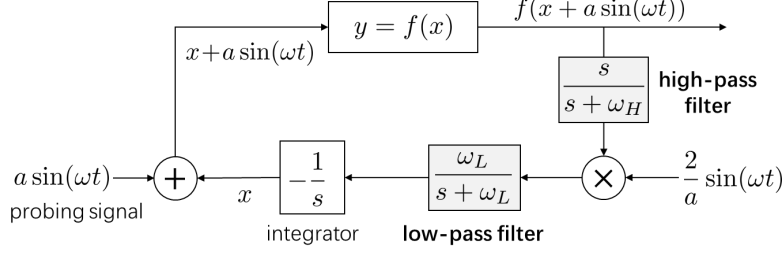


Figure 1: Block diagram of the extremum seeking system with a high-pass filter $\frac{s}{s+\omega_H}$ and a low-pass filter $\frac{\omega_L}{s+\omega_L}$ that solves $\min_x f(x)$.

for $\mathbf{x}, \mathbf{u} \in \mathbb{R}^d$ and $r > 0$, one can show that if \mathbf{u} is uniformly sampled from the unit sphere \mathbb{S}_{d-1} , then $G_f^{(1)}(\mathbf{x}; r, \mathbf{u})$ becomes an unbiased estimator of the gradient of a smoothed version of f [9]:¹

$$\mathbb{E}_{\mathbf{u} \sim \text{Unif}(\mathbb{S}_{d-1})} [G_f^{(1)}(\mathbf{x}; r, \mathbf{u})] = \nabla f_r(\mathbf{x}), \quad \text{where } f_r(\mathbf{x}) := \mathbb{E}_{\bar{\mathbf{u}} \sim \text{Unif}(\mathbb{B}_d)} [f(\mathbf{x} + r\bar{\mathbf{u}})].$$

By plugging the single-point gradient estimator $G_f^{(1)}(\mathbf{x}; r, \mathbf{u})$ into the gradient descent iterations for solving (1), we obtain the vanilla SZO method [9]:

$$\text{(Vanilla SZO)} : \quad \mathbf{x}_{k+1} = \mathbf{x}_k - \eta \cdot \frac{d}{r} f(\mathbf{x}_k + r\mathbf{u}_k) \mathbf{u}_k, \quad (3)$$

where $\{\mathbf{u}_k | k = 0, 1, 2, \dots\}$ are i.i.d. sampled from the uniform distribution $\text{Unif}(\mathbb{S}_{d-1})$. Here, $\eta > 0$ is the step size and parameter r is called the smoothing radius. One can show the convergence of (3) by appropriately choosing the step size η and the smoothing radius r under regular conditions.

The single-point gradient estimator (2) generally suffers from a high variance, which leads to slow convergence of the vanilla SZO method (3). To overcome this issue and achieve faster convergence, researchers have studied the two-point ZO methods [2], given by

$$\text{(Two-point ZO)} : \quad \mathbf{x}_{k+1} = \mathbf{x}_k - \eta \cdot \frac{d}{2r} (f(\mathbf{x}_k + r\mathbf{u}_k) - f(\mathbf{x}_k - r\mathbf{u}_k)) \mathbf{u}_k, \quad (4)$$

$$\text{or } \mathbf{x}_{k+1} = \mathbf{x}_k - \eta \cdot \frac{d}{r} (f(\mathbf{x}_k + r\mathbf{u}_k) - f(\mathbf{x}_k)) \mathbf{u}_k, \quad (5)$$

where two function evaluations are needed in each iteration. One can check that both of the two-point gradient estimators $\frac{d}{2r}(f(\mathbf{x} + r\mathbf{u}) - f(\mathbf{x} - r\mathbf{u}))\mathbf{u}$ and $\frac{d}{r}(f(\mathbf{x} + r\mathbf{u}) - f(\mathbf{x}))\mathbf{u}$ have the same expectation with the single-point gradient estimator $G_f^{(1)}(\mathbf{x}; r, \mathbf{u})$, but in general they have smaller variances and thus lead to faster convergence of two-point ZO methods.

2.2 Extremum Seeking Control

ES control for solving (the scalar version of) problem (1) is the continuous-time feedback closed-loop system illustrated in Figure 1. Instead of using random direction samples $r\mathbf{u}_k$ as in the ZO methods (3)-(5), the ES system adopts a sinusoidal probing signal $a \sin(\omega t)$ for function value perturbation, where $a > 0$ is the amplitude parameter and $\omega > 0$ is the frequency parameter. To analyze the ES system, we can first ignore the high-pass filter and the low-pass filter, since they are not essential to the system operation. As shown in Figure 1, a sinusoidal probing signal $a \sin(\omega t)$ is added to the state x , and the perturbed input $x + a \sin \omega t$ is fed into the static map $y = f(x)$. The output $y = f(x + a \sin(\omega t))$ is then multiplied with the signal $\frac{2}{a} \sin(\omega t)$ for correlation, and the loop is closed after passing through the integrator $-\frac{1}{s}$. Thus the ES system dynamics can be formulated as

$$\text{(Extremum seeking dynamics)} : \quad \dot{x} = -\frac{2}{a} f(x(t) + a \sin(\omega t)) \sin(\omega t), \quad (6)$$

¹Another choice of the distribution for the random direction \mathbf{u} is the Gaussian distribution $\mathcal{N}(\mathbf{0}, \mathbf{I}/d)$. We employ $\text{Unif}(\mathbb{S}_{d-1})$ in this paper for simplicity of exposition and theoretical analysis, while the results can be also extended to the Gaussian distribution case.

which is similar to the SZO method (3) in the formulation.

Rationale of ES Control. The rationale behind (6) is that when *parameter a is small and ω is large*, the ES dynamics (6) using only output feedback behaves approximately like the gradient descent flow $\dot{x} = -\nabla f(x)$, which can steer x to a (local) minimum $x^* \in \arg \min_x f(x)$ under appropriate conditions. Specifically, with a large value of ω , the ES dynamics (6) exhibits a timescale separation property, where the fast time variation is caused by the high-frequency sinusoidal signal $\sin(\omega t)$, while the slow variation induced by the integrator dominates the evolution of x . With a small value of a , we consider the Taylor expansion of the output $f(x + a \sin(\omega t))$ around x :

$$f(x + a \sin(\omega t)) = f(x) + a \sin(\omega t) \nabla f(x) + O(a).$$

Then one can compute the average dynamics of (6), which is given by $\dot{x} = -h_{\text{ave}}(x)$ and

$$\begin{aligned} h_{\text{ave}}(x) &:= \frac{1}{T} \int_0^T \frac{2}{a} f(x + a \sin(\omega t)) \sin(\omega t) dt \\ &= \frac{1}{T} \int_0^T \frac{2}{a} f(x) \sin(\omega t) + 2 \sin^2(\omega t) \nabla f(x) + O(a) dt = \nabla f(x) + O(a) \end{aligned} \quad (7)$$

with $T = \frac{2\pi}{\omega}$. Hence, the average dynamics of the ES system (6) with small a and large ω can be regarded as the gradient descent flow plus a small perturbation term $O(a)$. Besides, the ES control method can be easily extended to the multivariate case [6, 15] by using a probing signal vector $\sin(\omega t) = [\sin(\omega_1 t), \dots, \sin(\omega_d t)]^\top$ with $\omega_i \neq \omega_j$ for all $i \neq j$.

Rationale of High-Pass/Low-Pass Filters. As shown in Figure 1, a high-pass filter $\frac{s}{s+\omega_H}$ and a lower-pass filter $\frac{\omega_L}{s+\omega_L}$ are added to the ES system to improve the transient performance and mitigate oscillations, where ω_H and ω_L denote the cut-off frequencies. Intuitively, the high-pass filter works to wash out the constant and low-frequency components from the output $f(x + a \sin(\omega t))$. As indicated in the integral (7), the first term with slowly varying $f(x)$ is not useful and can be removed, while the second part with high-frequency $a \sin(\omega t) \nabla f(x)$ is critical to form the gradient estimation. In addition, before passing through the integrator, a clean and constant gradient estimate is desirable. Thus the low-pass filter is used to wash out high-frequency oscillations (induced by the sinusoidal probing signal) in the gradient estimation. See [20, 21] for more explanations.

3 Algorithm Design

In this section, we first present the proposed SZO algorithms with high-pass and low-pass filters, and then elaborate the derivation processes.

3.1 SZO Methods with High-Pass and Low-Pass Filters

We mimic the way that ES control applies the high-pass and low-pass filters and integrate them to the vanilla SZO method (3), which leads to the following new SZO algorithms.

1) By integrating a high-pass filter to (3), the new SZO method is formulated as (8) for $k = 1, 2, \dots$:

$$\text{(HF-SZO)} : \begin{cases} z_k = (1 - \beta)z_{k-1} + f(\mathbf{x}_k + r\mathbf{u}_k) - f(\mathbf{x}_{k-1} + r\mathbf{u}_{k-1}) \\ \mathbf{x}_{k+1} = \mathbf{x}_k - \eta \cdot \frac{d}{r} z_k \mathbf{u}_k \end{cases}, \quad (8)$$

where $\beta \geq 0$ is a parameter and $z_k \in \mathbb{R}$ is an intermediate variable with $z_0 := f(\mathbf{x}_0 + r\mathbf{u}_0)$. Interestingly, when setting parameter $\beta = 1$, the HF-SZO (8) becomes the residual-feedback SZO method proposed in [11]; and it reduces to the vanilla SZO method (3) when $\beta = 0$.

2) By integrating a low-pass filter to (3), the new SZO method is formulated as (9):

$$\text{(LF-SZO)} : \quad \mathbf{x}_{k+1} = \mathbf{x}_k - \eta \cdot \frac{d}{r} f(\mathbf{x}_k + r\mathbf{u}_k) \mathbf{u}_k + \alpha(\mathbf{x}_k - \mathbf{x}_{k-1}), \quad (9)$$

where $\alpha \in [0, 1]$ is a parameter. Compared with (3), a ‘‘momentum’’ term $\alpha(\mathbf{x}_k - \mathbf{x}_{k-1})$ is added to (9). When setting $\alpha = 0$, the LF-SZO (9) reduces to the vanilla SZO method (3).

3) By integrating both a high-pass filter and a low-pass filter to (3), the proposed HLF-SZO algorithm is formulated as (10):

$$\text{(HLF-SZO)} : \begin{cases} z_k = (1 - \beta)z_{k-1} + f(\mathbf{x}_k + r\mathbf{u}_k) - f(\mathbf{x}_{k-1} + r\mathbf{u}_{k-1}) \\ \mathbf{x}_{k+1} = \mathbf{x}_k - \eta \cdot \frac{d}{r} z_k \mathbf{u}_k + \alpha(\mathbf{x}_k - \mathbf{x}_{k-1}) \end{cases}, \quad (10)$$

which is basically the combination of (8) and (9). Note that in the HLF-SZO (10), only one function evaluation, i.e., $f(\mathbf{x}_k + r\mathbf{u}_k)$, is queried at each iteration, when the values $f(\mathbf{x}_{k-1} + r\mathbf{u}_{k-1})$ and \mathbf{x}_{k-1} are directly inherited from the last iteration.

It is surprising to find that *the integration of a high-pass filter coincides with the residual feedback method* proposed in [11], and *the integration of a low-pass filter can be interpreted as the momentum (heavy-ball) method* [18]. As for the choice of parameter β , the theoretical analysis in Section 4 shows that $\beta = 1$ is optimal for convergence, which is also validated by the numerical experiments conducted in Section 5. Besides, a momentum parameter $\alpha = 0.9$ or a similar value is usually suggested [1], and there have been extensive studies [18, 22, 23] on the role and selection of the momentum parameter. See Section 4 for more discussions.

3.2 Derivation Process

1) (*Adding a High-Pass Filter*). For the ES system illustrated in Figure 1, we denote f as the output of the static map and z as the signal after passing f through the high-pass filter $\frac{s}{s+\omega_H}$. Thus we have

$$\mathcal{L}\{z\} = \frac{s}{s+\omega_H}\mathcal{L}\{f\} \iff \dot{z} + \omega_H z = \dot{f}, \quad (11)$$

where $\mathcal{L}\{\cdot\}$ denotes the Laplacian transform. We discretize the dynamics (11) and obtain

$$\frac{z_k - z_{k-1}}{\delta} + \omega_H z_{k-1} = \frac{f_k - f_{k-1}}{\delta} \implies z_k = (1 - \delta\omega_H)z_{k-1} + f_k - f_{k-1}, \quad (12)$$

where $f_k := f(\mathbf{x}_k + r\mathbf{u}_k)$ and $\delta > 0$ is the discretization resolution. In this way, z_k can be interpreted as the refined value of f_k after passing through the high-pass filter. Denote $\beta := \delta\omega_H \geq 0$. Then substituting f_k by z_k in the vanilla SZO (3) leads to (8).

2) (*Adding a Low-Pass Filter*). As shown in Figure 1, a low-pass filter $\frac{\omega_L}{s+\omega_L}$ is added before passing the gradient estimation to the integrator. We denote $\mathbf{g} \in \mathbb{R}^d$ as the gradient estimation signal and $\mathbf{y} \in \mathbb{R}^d$ as the refined signal after passing \mathbf{g} through the low-pass filter. Thus we have the relation:

$$\mathcal{L}\{\mathbf{y}\} = \frac{\omega_L}{s+\omega_L}\mathcal{L}\{\mathbf{g}\} \iff \dot{\mathbf{y}} = \omega_L(-\mathbf{y} + \mathbf{g}). \quad (13)$$

We discretize the resultant dynamics (13) and the integrator dynamics $\dot{\mathbf{x}} = -\mathbf{y}$, which leads to

$$\frac{\mathbf{y}_{k+1} - \mathbf{y}_k}{\delta} = \omega_L(-\mathbf{y}_k + \mathbf{g}_k) \implies \mathbf{y}_{k+1} = (1 - \delta\omega_L)\mathbf{y}_k + \delta\omega_L\mathbf{g}_k, \quad (14a)$$

$$\frac{\mathbf{x}_{k+1} - \mathbf{x}_k}{\delta} = -\mathbf{y}_{k+1} \implies \mathbf{x}_{k+1} = \mathbf{x}_k - \delta\mathbf{y}_{k+1}. \quad (14b)$$

Denote $\eta := \delta^2\omega_L$ and $\alpha := 1 - \delta\omega_L$. With $\mathbf{g}_k = \frac{d}{r}f(\mathbf{x}_k + r\mathbf{u}_k)\mathbf{u}_k$ in the vanilla SZO (3), we obtain (9) after eliminating the variable \mathbf{y} from (14).

3) (*Adding Both High-Pass and Low-Pass Filters*). When both high-pass and low-pass filters are applied, the resultant method is the combination of (12) and (14), which leads to (10).

4 Theoretic Analysis

We make the following assumption throughout our analysis.

Assumption 1. *The function f is G -Lipschitz and L -smooth, i.e., for all $\mathbf{x}, \mathbf{y} \in \mathbb{R}^d$, we have*

$$\|f(\mathbf{x}) - f(\mathbf{y})\| \leq G\|\mathbf{x} - \mathbf{y}\|, \quad \|\nabla f(\mathbf{x}) - \nabla f(\mathbf{y})\| \leq L\|\mathbf{x} - \mathbf{y}\|.$$

We first analyze the convergence of HLF-SZO (10) for the **convex case**.

Theorem 1. (*Convex Case*). *Let $\alpha \in [0, 1)$ and $\beta \in (0, 2)$. Suppose that f is convex and has a minimizer $\mathbf{x}^* \in \mathbb{R}^d$, and let the total number of iterations T be given. Then by choosing*

$$\eta \leq \frac{(1-\alpha)(1-|\beta|)^2}{25LdT^{1/3}}, \quad \frac{4\eta dG}{(1-|\beta|)(1-\alpha)} \leq r \leq \frac{G}{LT^{1/3}}, \quad (15)$$

we can achieve

$$\mathbb{E}[f(\bar{\mathbf{x}}_T)] - f(\mathbf{x}^*) \leq \frac{3(1-\alpha)\|\mathbf{x}_1 - \mathbf{x}^*\|^2}{4\eta T} + \frac{3G^2}{4LT^{2/3}} + O(d/T),$$

where $\bar{\mathbf{x}}_T := \frac{1}{T} \sum_{k=1}^T \mathbf{x}_k$. Furthermore, by letting η achieves the equality in (15), we have

$$\mathbb{E}[f(\bar{\mathbf{x}}_T)] - f(\mathbf{x}^*) \leq \frac{d}{T^{2/3}} \left(\frac{75L\|\mathbf{x}_1 - \mathbf{x}^*\|^2}{4(1-|\beta|)^2} + \frac{3G^2}{4Ld} \right) + O(d/T). \quad (16)$$

The proof of Theorem 1 is given in Appendix B. Some implications and discussions of Theorem 1 are presented as follows:

1. **Convergence rate:** It is seen that the leading term on the right-hand side of (16) is $O(d/T^{2/3})$. This convergence rate has the same dependence on T as the residual-feedback SZO method given in [11] for the convex and smooth case, but achieves better dependence on the problem dimension d , which is due to refined analysis on the second moment of the zeroth-order gradient estimator. On the other hand, this convergence rate is inferior to the ZO method with a two-point gradient estimator [2], which achieves a convergence rate of $O(d/T)$.

2. **Choice of β :** It is seen that the optimal β that minimizes the leading term in (16) is given by $\beta = 1$. We shall see that this choice implied by our theoretical analysis is in accordance with our empirical results in Section 5. As mentioned above, the HF-SZO (8) with $\beta = 1$ is equivalent to the residual-feedback SZO method [11].

3. **Choice of α :** It is seen that the parameter α does not appear in the leading term on the right-hand side of (16). This indicates that theoretically, the convergence of HLF-SZO (10) is at least as fast as HF-SZO (8). On the other hand, we shall see in Section 5 that HLF-SZO (10) with $\alpha > 0$ can achieve faster convergence than HF-SZO (8). One possible reason for the better empirical convergence behavior is that the upper bound on the step size η given by (15) is proportional to $1 - \alpha$, which is conservative, and in practice, a larger step size can be employed to facilitate convergence.

Next, we establish the convergence of HLF-SZO (10) for the **nonconvex case**.

Theorem 2. (Nonconvex Case). Let $\alpha \in [0, 1)$ and $\beta \in (0, 2)$. Suppose $f^* := \inf_{x \in \mathbb{R}^d} f(x) > -\infty$, and let the total number of iterations T be sufficiently large. Then by choosing

$$\eta \leq \frac{(1-\alpha)(1-|\beta|)^2}{25LdT^{1/3}}, \quad \frac{4\eta dG}{(1-|\beta|)(1-\alpha)} \leq r \leq \frac{G}{LT^{1/3}}, \quad (15)$$

we can achieve

$$\frac{1}{T} \sum_{k=1}^T \mathbb{E}[\|\nabla f(\mathbf{x}_k)\|^2] \leq \frac{4(1-\alpha)(f(\mathbf{x}_1) - f^*)}{\eta T} + \frac{8G^2}{T^{2/3}} + O(d/T).$$

Furthermore, by letting η achieves the equality in (15), we have

$$\frac{1}{T} \sum_{k=1}^T \mathbb{E}[\|\nabla f(\mathbf{x}_k)\|^2] \leq \frac{d}{T^{2/3}} \left(\frac{100L(f(\mathbf{x}_1) - f^*)}{(1-|\beta|)^2} + \frac{8G^2}{d} \right) + O(d/T). \quad (17)$$

The proof of Theorem 2 is provided in Appendix C. Note that we use the ergodic rate of the squared norm of the gradient $\|\nabla f(\mathbf{x}_k)\|^2$ to characterize the convergence behavior, which is common for local methods of unconstrained smooth nonconvex problems where we do not aim for global optimal solutions [24, 2]. On the other hand, we can see that the bound (17) is very similar to (16), indicating that much of the discussions on Theorem 1 will also apply to the smooth nonconvex case with minor modifications.

5 Numerical Experiments

In this section, we first conduct numerical experiments to study the properties of the SZO methods with high-pass and low-pass filters. Then the performance of the proposed HLF-SZO algorithm is demonstrated on logistic regression, ridge regression, and two artificial test functions, compared with the residual-feedback SZO and two-point ZO method.

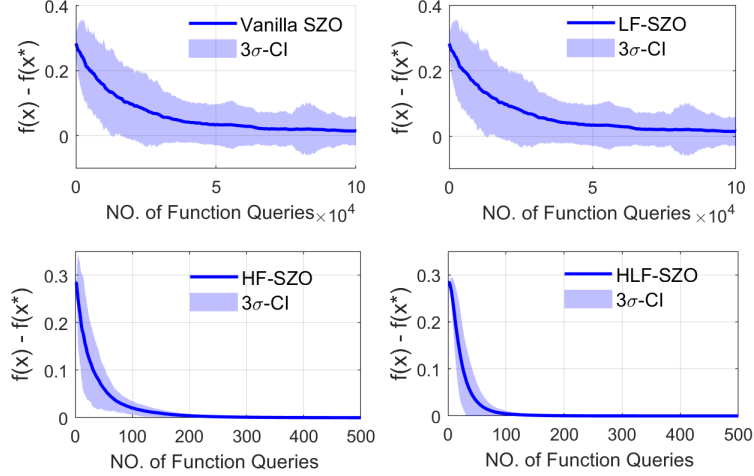


Figure 2: The convergence results of applying the vanilla SZO (3), HF-SZO (8), LF-SZO (9), and HLF-SZO (10) to solve the logistic regression (18) in Case 1.1a.

5.1 Properties of SZO Methods with High-Pass/Low-Pass Filters

This subsection demonstrates the performance comparison among vanilla SZO (3), HF-SZO (8), LF-SZO (9), and HLF-SZO (10) methods, and studies the impact of the parameter β on HLF-SZO (10), through the numerical tests on logistic regression and ridge regression.

We consider the following four cases. For each case, we run each ZO method 200 times and calculate its mean and 3σ -confidence interval (CI) of the distance to optimality, i.e., $f(\mathbf{x}_k) - f(\mathbf{x}^*)$.

1) Logistic Regression. Consider solving the logistic regression problem (18) [25]:

$$\min_{\mathbf{x} \in \mathbb{R}^d} f(\mathbf{x}) = \frac{1}{N} \sum_{i=1}^N \log(1 + \exp(-y_i \cdot A_i^\top \mathbf{x})), \quad (18)$$

where $A_i \in \mathbb{R}^d$ is one of the data samples, $y_i \in \{-1, 1\}$ is the corresponding class label, and N is the total sample size. In our experiments, each element of a data sample A_i is randomly and independently generated from the uniform distribution $\text{Unif}([-1, 1])$, and the label is computed as $y_i = \text{sign}(A_i^\top \mathbf{x}_* + \epsilon_i)$ with $\mathbf{x}_* = 0.5\mathbf{1}_d$ and $\epsilon_i \sim \text{Unif}([-0.5, 0.5])$.

Case 1.1a) Comparison among SZO methods on logistic regression: Consider a small case with $d = 2$ and $N = 20$. For the SZO methods (3) (8), (9), and (10), we set $r = 0.1$, $\beta = 1$, $\alpha = 0.9$ and initial condition $\mathbf{x}_0 = \mathbf{0}_d$. We manually optimize the stepsize η of each method to achieve the fastest convergence². The selected stepsizes are 5×10^{-4} , 0.3 , 5×10^{-5} , and 0.05 for the vanilla SZO (3), HF-SZO (8), LF-SZO (9), and HLF-SZO (10), respectively. Figure 2 illustrates the experimental results of solving the logistic regression (18) with these SZO methods.

Case 1.1b) Impact of Coefficient β on logistic regression: Then we tune the coefficient β from 0.6 to 1.4 and run experiments for each case to study the impact of β . Other settings are the same as the above case 1.1a). The convergence results of HLF-SZO (10) with different β are shown in Figure 3.

2) Ridge Regression. Consider solving the ridge regression problem [25]:

$$\min_{\mathbf{x} \in \mathbb{R}^d} f(\mathbf{x}) = \frac{1}{2} \|\mathbf{b} - H\mathbf{x}\|_2^2 + \frac{1}{2} c \|\mathbf{x}\|_2^2. \quad (19)$$

In our experiments, each entry of matrix $H \in \mathbb{R}^{N \times d}$ is generated randomly and independently from Gaussian distribution $\mathcal{N}(0, 1)$. The vector $\mathbf{b} \in \mathbb{R}^N$ is constructed by letting $\mathbf{b} = H\mathbf{x}_* + \epsilon$ for a certain predefined $\mathbf{x}_* \in \mathbb{R}^d$ and $\epsilon \sim \mathcal{N}(\mathbf{0}, 0.1\mathbf{I})$. The regularization constant is set to be $c = 0.1$.

²We gradually increase the stepsize for each method and select the one with the fastest convergence without divergence.

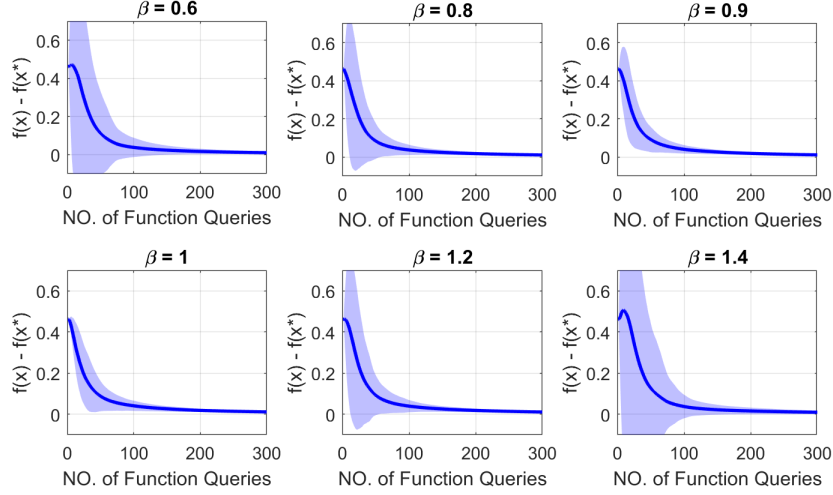


Figure 3: The convergence results of HLF-SZO (10) under different β for solving the logistic regression (18) in Case 1.1b.

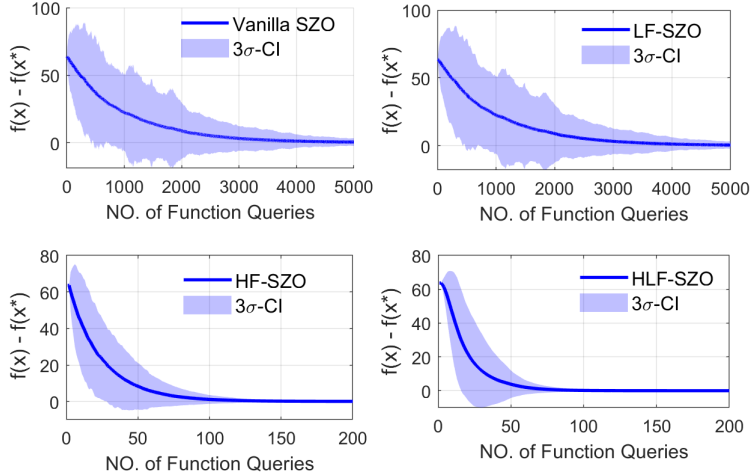


Figure 4: The convergence results of applying the vanilla SZO (3), HF-SZO (8), LF-SZO (9), and HLF-SZO (10) to solve the ridge regression (19) in Case 1.2a.

Case 1.2a) Comparison among SZO methods on ridge regression: Consider a small case with $d = 5$, $N = 100$ and $x_* = 0.51_d$. For the SZO methods (3) (8), (9), and (10), we set $r = 0.1$, $\beta = 1$, $\alpha = 0.9$ and initial condition $x_0 = \mathbf{0}_d$. We manually optimize the stepsize η of each method to achieve the fastest convergence. The selected stepsizes are 6×10^{-6} , 2.5×10^{-4} , 6×10^{-7} , and 6×10^{-5} for the vanilla SZO (3), HF-SZO (8), LF-SZO (9), and HLF-SZO (10), respectively. Figure 4 illustrates the experimental results of solving the ridge regression (19) with these SZO methods.

Case 1.2b) Impact of Coefficient β on ridge regression: Consider a larger-scale problem with $d = 50$, $N = 1000$ and $x_* = \mathbf{1}_d$. For the HLF-SZO method (10), we set $r = 0.1$, $\alpha = 0.9$, $\eta = 1 \times 10^{-7}$, and initial condition $x_0 = \mathbf{0}_d$. Then we tune the coefficient β from 0.6 to 1.4 and run experiments for each case to study the impact of β . The convergence results of HLF-SZO (10) with different β are illustrated as Figure 5.

The key observations are summarized as follows:

- 1) From Figures 2 and 4, it is seen that the variances of HF-SZO and HLF-SZO are much smaller than the vanilla SZO and LF-SZO due to the application of the high-pass filter, and thus HF-SZO

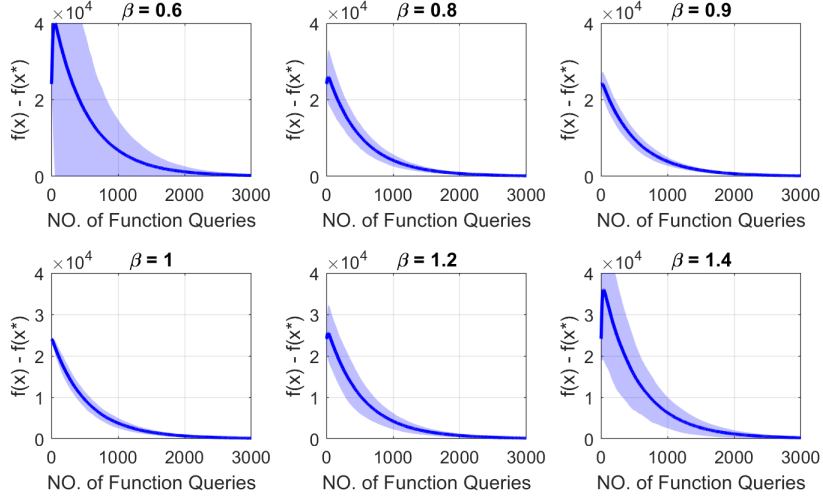


Figure 5: The convergence results of HLF-SZO (10) under different β for solving the ridge regression (19) in Case 1.2b.

and HLF-SZO can achieve much faster convergence. It indicates that the high-pass filter can significantly reduce the variance of SZO.

- 2) In addition, from Figures 2 and 4, it is seen that HLF-SZO can achieve faster convergence than HF-SZO due to the application of the low-pass filter. This will be further studied in the next subsection with more experiments.
- 3) From Figures 3 and 5, it is observed that the case with $\beta = 1$ achieves the least variance and fastest convergence, which is consistent with the theoretical analysis in Section 4 that $\beta = 1$ is the optimal choice.

5.2 Comparison with State-of-The-Art ZO Algorithms

This subsection compares the performance of the proposed HLF-SZO method (10) with the state-of-the-art residual-feedback SZO method [11] and the two-point ZO method (4). Note that the residual-feedback SZO method is equivalent to the HF-SZO method (8) with $\beta = 1$. Besides, the vanilla SZO method (3) is not considered for comparison, as it has much slower convergence and a much larger variance. In particular, we test these ZO algorithms on logistic regression, ridge regression, and two artificial test functions.

1) Regression Problems:

Case 2.1a) Solving the **logistic regression** problem (18) with $d = 50$ and $N = 1000$. We manually optimize the stepsize η to achieve the fastest convergence, and the selected stepsizes are 1.5×10^{-2} , 4.5×10^{-2} , and 0.7 for the HLF-SZO (10), the residual-feedback SZO, and the two-point ZO (4). Other settings are the same as Section 5.1. The convergence comparison is illustrated in Figure 6.

Case 2.1b) Solving the **ridge regression** problem (19) with $d = 50$, $N = 1000$ and $\mathbf{x}_* = \mathbf{1}_d$. For the ZO algorithms, we set $r = 0.1$, $\alpha = 0.9$, $\beta = 1$, and manually optimize the stepsize η to achieve the fastest convergence. The selected stepsizes are 1×10^{-6} , 2.4×10^{-6} , and 2×10^{-5} for the HLF-SZO (10), the residual-feedback SZO, and two-point ZO (4), respectively. Other settings are the same as Section 5.1. Figure 6 shows the convergence comparison for solving the ridge regression problem (19).

2) Test Functions:

Case 2.2a) Minimizing the nonconvex **Beale function**³ given by (20), which is an artificial test function and has a global minimum at $\mathbf{x}^* = [3; 0.5]$ with $f(\mathbf{x}^*) = 0$.

$$f(\mathbf{x}) = (1.5 - x_1 + x_1x_2)^2 + (2.25 - x_1 + x_1x_2^2)^2 + (2.625 - x_1 + x_1x_2^3)^2. \quad (20)$$

³Beale function: <https://www.sfu.ca/~ssurjano/beale.html>.

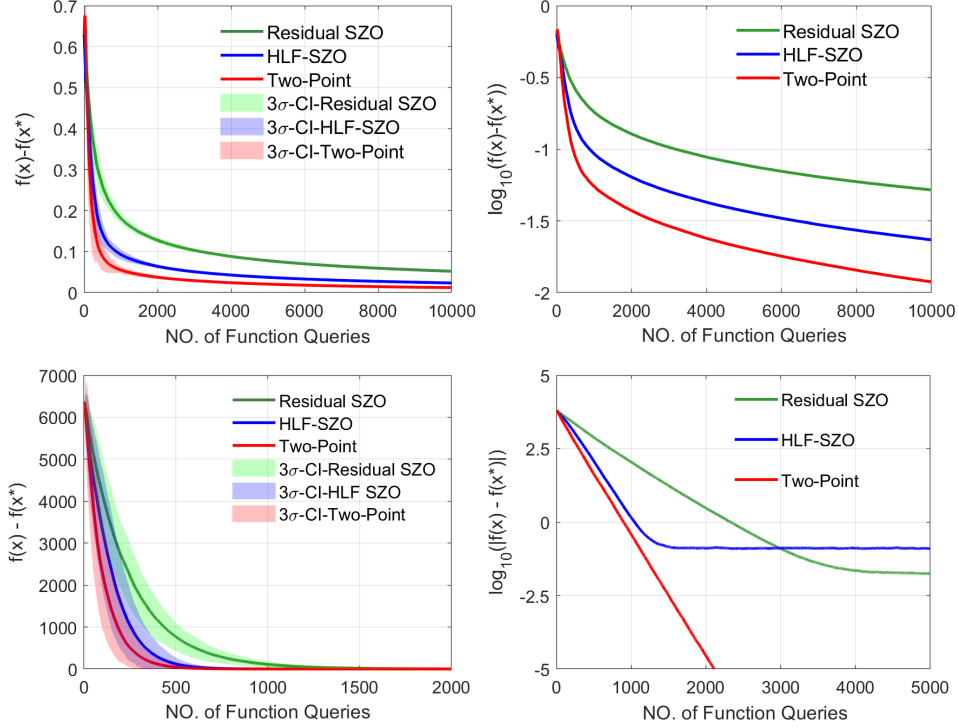


Figure 6: The convergence comparison of applying the residual-feedback SZO, HLF-SZO (10), and two-point ZO (4) to solve the regression problems. (The upper two plots are for the **logistic regression** (18) in Case 2.1a, and the lower two plots are for the **ridge regression** (19) in case 2.1b.)

For the ZO algorithms, we set $r = 0.01$, $\beta = 1$, $\alpha = 0.9$, $\mathbf{x}_0 = [0; 0]$, and manually optimize the stepsize η to achieve the fastest convergence. The selected stepsizes are 2×10^{-4} , 5×10^{-4} , and 6×10^{-3} for the HLF-SZO (10), the residual-feedback SZO, and the two-point ZO (4), respectively. Figure 7 illustrates the convergence comparison for minimizing the Beale function (20).

Case 2.2b) Minimizing the nonconvex **Matyas function** given by (21), which has a global minimum at $\mathbf{x}^* = [0; 0]$ with $f(\mathbf{x}^*) = 0$.

$$f(\mathbf{x}) = 0.26(x_1^2 + x_2^2) - 0.48x_1x_2. \quad (21)$$

The initial condition is $\mathbf{x}_0 = [-5; -5]$, and other settings are the same as Case 2.2a. After manual optimization, the selected stepsizes are 7×10^{-3} , 2×10^{-2} , and 0.5 for the HLF-SZO (10), the residual-feedback SZO, and the two-point ZO (4), respectively. Figure 7 illustrates the convergence comparison for minimizing the Matyas function (21).

From Figures 6 and 7, it is observed that the HLF-SZO can achieve faster convergence than the residual-feedback SZO method in all cases, although not as fast as the two-point method. It implies that the integration of a low-pass filter can effectively accelerate the convergence of SZO via the momentum term.

6 Conclusion

This work leverages the high-pass and low-pass filters from ES control to improve the performance of SZO. By integrating a high-pass filter and a low-pass filter to the vanilla SZO method, we develop a novel SZO algorithm named HLF-SZO. It is surprising to find that the integration of a high-pass filter coincides with the residual-feedback SZO method in [11], and the integration of a low-pass filter can be interpreted as the momentum method. We prove that the proposed HLF-SZO algorithm achieves a convergence rate of $O(d/T^{\frac{2}{3}})$ for Lipschitz and smooth problems (in both convex and nonconvex cases), which is better than the convergence rate $O(d^2/T^{\frac{2}{3}})$ of residual-feedback SZO provided in

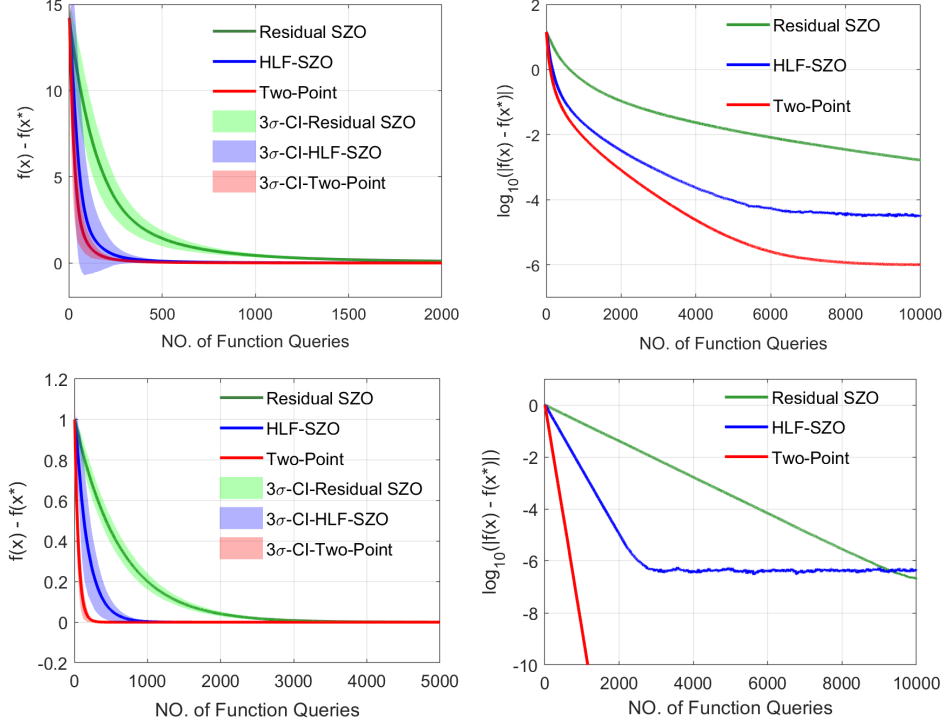


Figure 7: The convergence comparison of applying the residual-feedback SZO, HLF-SZO (10), and two-point ZO (4) to minimize the test functions. (The upper two plots are for the **Beale function** (20) in Case 2.2a, and the lower two plots are for the **Matyas function** (21) in Case 2.2b.)

[11] and inferior to the two-point ZO with a convergence rate of $O(d/T)$. Numerical experiments demonstrate that the high-pass filter can significantly reduce the variance and the low-pass filter can accelerate the convergence. As a result, the proposed HLF-SZO algorithm has a much smaller variance and much faster convergence than the vanilla SZO method, and empirically outperforms the residual-feedback SZO method. This enables the application of HLF-SZO to practical black-box optimization and simulation-based learning and control problems.

This work bridges ZO in the optimization community and ES control in the control community, and shows that useful tools from ES control can be borrowed to benefit ZO. Our work is a preliminary attempt in this direction and there is much more to study. For example, 1) this work only adopts the simplest high-pass/low-pass filters and time discretization method, and better designs of the filters and discretization schemes may lead to further improvement; 2) this work focuses on the deterministic case, and we are working on the extension of the HLF-SZO algorithm to stochastic optimization with stochastic gradient descent (SGD) methods.

References

- [1] Sebastian Ruder. An overview of gradient descent optimization algorithms. *arXiv preprint arXiv:1609.04747*, 2016.
- [2] Yurii Nesterov and Vladimir Spokoiny. Random gradient-free minimization of convex functions. *Foundations of Computational Mathematics*, 17(2):527–566, 2017.
- [3] Dhruv Malik, Ashwin Pananjady, Kush Bhatia, Koulik Khamaru, Peter Bartlett, and Martin Wainwright. Derivative-free methods for policy optimization: Guarantees for linear quadratic systems. In *The 22nd International Conference on Artificial Intelligence and Statistics*, pages 2916–2925. PMLR, 2019.
- [4] Yingying Li, Yujie Tang, Runyu Zhang, and Na Li. Distributed reinforcement learning for decentralized linear quadratic control: A derivative-free policy optimization approach. *arXiv preprint arXiv:1912.09135*, 2019.

- [5] Pin-Yu Chen, Huan Zhang, Yash Sharma, Jinfeng Yi, and Cho-Jui Hsieh. Zoo: Zeroth order optimization based black-box attacks to deep neural networks without training substitute models. In *Proceedings of the 10th ACM workshop on artificial intelligence and security*, pages 15–26, 2017.
- [6] Xin Chen, Jorge I Poveda, and Na Li. Model-free optimal voltage control via continuous-time zeroth-order methods. *arXiv preprint arXiv:2103.14703*, 2021.
- [7] Yue Chen, Andrey Bernstein, Adithya Devraj, and Sean Meyn. Model-free primal-dual methods for network optimization with application to real-time optimal power flow. In *2020 American Control Conference (ACC)*, pages 3140–3147. IEEE, 2020.
- [8] Sijia Liu, Pin-Yu Chen, Bhavya Kailkhura, Gaoyuan Zhang, Alfred O Hero III, and Pramod K Varshney. A primer on zeroth-order optimization in signal processing and machine learning: Principals, recent advances, and applications. *IEEE Signal Processing Magazine*, 37(5):43–54, 2020.
- [9] Abraham D. Flaxman, Adam Tauman Kalai, and H. Brendan McMahan. Online convex optimization in the bandit setting: Gradient descent without a gradient. In *Proceedings of the Sixteenth Annual ACM-SIAM Symposium on Discrete Algorithms*, page 385–394, 2005.
- [10] Ohad Shamir. An optimal algorithm for bandit and zero-order convex optimization with two-point feedback. *The Journal of Machine Learning Research*, 18(1):1703–1713, 2017.
- [11] Yan Zhang, Yi Zhou, Kaiyi Ji, and Michael M Zavlanos. Improving the convergence rate of one-point zeroth-order optimization using residual feedback. *arXiv preprint arXiv:2006.10820*, 2020.
- [12] Ofer Dekel, Ronen Eldan, and Tomer Koren. Bandit smooth convex optimization: Improving the bias-variance tradeoff. In *NIPS*, pages 2926–2934, 2015.
- [13] Ankan Saha and Ambuj Tewari. Improved regret guarantees for online smooth convex optimization with bandit feedback. In *Proceedings of the Fourteenth International Conference on Artificial Intelligence and Statistics*, pages 636–642. JMLR Workshop and Conference Proceedings, 2011.
- [14] Kartik B Ariyur and Miroslav Krstić. *Real Time Optimization by Extremum Seeking Control*. Wiley Online Library, 2003.
- [15] Jorge I. Poveda and Na Li. Robust hybrid zero-order optimization algorithms with acceleration via averaging in time. *Automatica*, 123:109361, 2021.
- [16] Hans-Bernd Dürr, Chen Zeng, and Christian Ebenbauer. Saddle point seeking for convex optimization problems. *IFAC Proceedings Volumes*, 46(23):540–545, 2013.
- [17] Maojiao Ye and Guoqiang Hu. Distributed extremum seeking for constrained networked optimization and its application to energy consumption control in smart grid. *IEEE Transactions on Control Systems Technology*, 24(6):2048–2058, 2016.
- [18] Boris T Polyak. Some methods of speeding up the convergence of iteration methods. *Ussr computational mathematics and mathematical physics*, 4(5):1–17, 1964.
- [19] Miroslav Krstić. Performance improvement and limitations in extremum seeking control. *Systems & Control Letters*, 39(5):313–326, 2000.
- [20] Ying Tan, William H Moase, Chris Manzie, Dragan Nešić, and Iven MY Mareels. Extremum seeking from 1922 to 2010. In *Proceedings of the 29th Chinese control conference*, pages 14–26. IEEE, 2010.
- [21] Ying Tan, Dragan Nešić, and Iven Mareels. On non-local stability properties of extremum seeking control. *Automatica*, 42(6):889–903, 2006.
- [22] Wei Tao, Sheng Long, Gaowei Wu, and Qing Tao. The role of momentum parameters in the optimal convergence of adaptive polyak’s heavy-ball methods. *arXiv preprint arXiv:2102.07314*, 2021.
- [23] Ning Qian. On the momentum term in gradient descent learning algorithms. *Neural networks*, 12(1):145–151, 1999.
- [24] Saeed Ghadimi and Guanghui Lan. Stochastic first-and zeroth-order methods for nonconvex stochastic programming. *SIAM Journal on Optimization*, 23(4):2341–2368, 2013.

- [25] César A Uribe, Soomin Lee, Alexander Gasnikov, and Angelia Nedić. A dual approach for optimal algorithms in distributed optimization over networks. In *2020 Information Theory and Applications Workshop (ITA)*, pages 1–37. IEEE, 2020.
- [26] Yurii Nesterov. *Introductory Lectures on Convex Optimization: A Basic Course*. Springer Science+Business Media, LLC, 2004.

A Notations and Preliminary Results

We let \mathcal{F}_k denote the filtration generated by $\mathbf{x}_1, \dots, \mathbf{x}_k$ and $\mathbf{u}_1, \dots, \mathbf{u}_{k-1}$. It can be checked that the iterations can be equivalently written as

$$\begin{aligned} \mathbf{g}_k &= \frac{d}{r} z_k \mathbf{u}_k, \quad z_k = \begin{cases} \frac{1}{2}(f(\mathbf{x}_k + r\mathbf{u}_k) - f(\mathbf{x}_k - r\mathbf{u}_k)), & k = 1, \\ (1 - \beta)z_{k-1} + f(\mathbf{x}_k + r\mathbf{u}_k) - f(\mathbf{x}_{k-1} + r\mathbf{u}_{k-1}), & k > 1, \end{cases} \\ \mathbf{p}_k &= \alpha \mathbf{p}_{k-1} + \eta \mathbf{g}_k, \\ \mathbf{x}_{k+1} &= \mathbf{x}_k - \mathbf{p}_k, \end{aligned}$$

for $k \geq 1$, and we set $\mathbf{p}_0 = \mathbf{0}$ and $\mathbf{x}_0 = \mathbf{x}_1$. We denote $\tilde{\beta} := 1 - |1 - \beta|$ for notational simplicity.

The following lemma deals with the expectation of \mathbf{g}_k .

Lemma 1. *Denote $\mathbb{B}_d := \{x \in \mathbb{R}^d : \|x\| \leq 1\}$. For all $k \geq 1$, we have*

$$\mathbb{E}[\mathbf{g}_k | \mathcal{F}_k] = \nabla f_r(\mathbf{x}_k),$$

where $f_r : \mathbb{R}^d \rightarrow \mathbb{R}$ is defined by $f_r(\mathbf{x}) := \mathbb{E}_{\mathbf{y} \sim \text{Unif}(\mathbb{B}_d)}[f(\mathbf{x} + r\mathbf{y})]$. Moreover, for all $\mathbf{x} \in \mathbb{R}^d$,

$$|f_r(\mathbf{x}) - f(\mathbf{x})| \leq \frac{1}{2} L r^2, \quad \|\nabla f_r(\mathbf{x}) - \nabla f(\mathbf{x})\| \leq L r,$$

and if f is convex, then $f_r(\mathbf{x}) \geq f(\mathbf{x})$.

Proof. The result $\mathbb{E}[\mathbf{g}_k | \mathcal{F}_k] = \nabla f_r(\mathbf{x}_k)$ is standard in zeroth-order optimization [9]. By the L -smoothness of f , we have

$$r \langle \mathbf{y}, \nabla f(\mathbf{x}) \rangle - \frac{L}{2} r^2 \|\mathbf{y}\|^2 \leq f(\mathbf{x} + r\mathbf{y}) - f(\mathbf{x}) \leq r \langle \mathbf{y}, \nabla f(\mathbf{x}) \rangle + \frac{L}{2} r^2 \|\mathbf{y}\|^2,$$

and by taking the expectation with $\mathbf{y} \sim \text{Unif}(\mathbb{B}_d)$, we get

$$-\frac{L}{2} r^2 \leq f_r(\mathbf{x}) - f(\mathbf{x}) \leq \frac{L}{2} r^2$$

for any $\mathbf{x} \in \mathbb{R}^d$. If f is convex, then $f(\mathbf{x} + r\mathbf{y}) - f(\mathbf{x}) \geq r \langle \mathbf{y}, \nabla f(\mathbf{x}) \rangle$, and by taking the expectation with $\mathbf{y} \sim \text{Unif}(\mathbb{B}_d)$, we get $f_r(\mathbf{x}) \geq f(\mathbf{x})$.

Finally, regarding the gradient $\nabla f_r(\mathbf{x})$, we have

$$\begin{aligned} \|\nabla f_r(\mathbf{x}) - \nabla f(\mathbf{x})\| &= \|\nabla \mathbb{E}_{\mathbf{y} \sim \text{Unif}(\mathbb{B}_d)}[f(\mathbf{x} + r\mathbf{y})] - \nabla f(\mathbf{x})\| \\ &= \|\mathbb{E}_{\mathbf{y} \sim \text{Unif}(\mathbb{B}_d)}[\nabla f(\mathbf{x} + r\mathbf{y}) - \nabla f(\mathbf{x})]\| \\ &\leq \mathbb{E}_{\mathbf{y} \sim \text{Unif}(\mathbb{B}_d)}[Lr \|\mathbf{y}\|] \leq Lr, \end{aligned}$$

where we interchange integration and differentiation in the second step, which can be justified by the dominated convergence theorem. \square

The following lemma deals with the accumulated second moment of z_k .

Lemma 2. *We have*

$$\sum_{k=1}^T \mathbb{E}[|z_k|^2] \leq \frac{25r^2}{4\tilde{\beta}^2 d} \sum_{k=1}^{T-1} \mathbb{E}[\|\nabla f(\mathbf{x}_{k-1})\|^2] + \frac{2G^2}{\tilde{\beta}^2} \sum_{k=1}^{T-1} \mathbb{E}[\|\mathbf{p}_{k-1}\|^2] + \frac{10Tr^4 L^2}{\tilde{\beta}^2}.$$

Proof. For $k = 1$, we have

$$\begin{aligned} \mathbb{E}[|z_k|^2] &= \mathbb{E}\left[\left|\frac{f(\mathbf{x}_k + r\mathbf{u}_k) - f(\mathbf{x}_k - r\mathbf{u}_k)}{2}\right|^2\right] \\ &= \mathbb{E}\left[\left\langle r \nabla f(\mathbf{x}_k), \mathbf{u}_k \right\rangle + \frac{1}{2} \int_{-r}^r \langle \nabla f(\mathbf{x}_k + s\mathbf{u}_k) - \nabla f(\mathbf{x}_k), \mathbf{u}_k \rangle ds \right]^2 \end{aligned}$$

$$\begin{aligned}
&\leq \frac{5}{4} \mathbb{E} [r^2 \nabla f(\mathbf{x}_k)^\top \mathbb{E} [\mathbf{u}_k \mathbf{u}_k^\top | \mathcal{F}_k] \nabla f(\mathbf{x}_k)] \\
&\quad + 5 \mathbb{E} \left[\frac{1}{4} \left| \int_{-r}^r \|\nabla f(\mathbf{x}_k + s\mathbf{u}_k) - \nabla f(\mathbf{x}_k)\| \|\mathbf{u}_k\| ds \right|^2 \right] \\
&\leq \frac{5r^2}{4d} \mathbb{E} [\|\nabla f(\mathbf{x}_k)\|^2] + \frac{5}{4} \mathbb{E} \left[\left| \int_{-r}^r L|s| \|\mathbf{u}_k\|^2 ds \right|^2 \right] \leq \frac{5r^2}{4d} \mathbb{E} [\|\nabla f(\mathbf{x}_k)\|^2] + \frac{5}{4} L^2 r^4.
\end{aligned}$$

Then for $k > 1$, we get

$$\begin{aligned}
\mathbb{E} [|z_k|^2] &\leq \frac{1}{|1-\beta|} \cdot (1-\beta)^2 \mathbb{E} [|z_{k-1}|^2] + \frac{1}{1-|\beta|} \mathbb{E} [|f(\mathbf{x}_k + r\mathbf{u}_k) - f(\mathbf{x}_{k-1} + r\mathbf{u}_{k-1})|^2] \\
&= (1-\tilde{\beta}) \mathbb{E} [|z_{k-1}|^2] + \tilde{\beta}^{-1} \mathbb{E} [|f(\mathbf{x}_k + r\mathbf{u}_k) - f(\mathbf{x}_{k-1} + r\mathbf{u}_{k-1})|^2]
\end{aligned}$$

when $\beta \neq 1$, and obviously this inequality also extends to the $\beta = 1$ case. Furthermore,

$$\begin{aligned}
\mathbb{E} [|f(\mathbf{x}_k + r\mathbf{u}_k) - f(\mathbf{x}_{k-1} - r\mathbf{u}_{k-1})|^2] &\leq 2 \left(\mathbb{E} [|f(\mathbf{x}_{k-1} + r\mathbf{u}_k) - f(\mathbf{x}_{k-1} + r\mathbf{u}_{k-1})|^2] \right. \\
&\quad \left. + \mathbb{E} [|f(\mathbf{x}_k + r\mathbf{u}_k) - f(\mathbf{x}_{k-1} + r\mathbf{u}_k)|^2] \right).
\end{aligned}$$

For the first term, we have

$$\begin{aligned}
&\mathbb{E} [|f(\mathbf{x}_{k-1} + r\mathbf{u}_k) - f(\mathbf{x}_{k-1} + r\mathbf{u}_{k-1})|^2] \\
&= \mathbb{E} \left[\left| r \langle \nabla f(\mathbf{x}_{k-1}), \mathbf{u}_k - \mathbf{u}_{k-1} \rangle + \int_0^r \langle \nabla f(\mathbf{x}_{k-1} + s\mathbf{u}_k) - \nabla f(\mathbf{x}_{k-1}), \mathbf{u}_k \rangle ds \right. \right. \\
&\quad \left. \left. - \int_0^r \langle \nabla f(\mathbf{x}_{k-1} + s\mathbf{u}_{k-1}) - \nabla f(\mathbf{x}_{k-1}), \mathbf{u}_{k-1} \rangle ds \right|^2 \right] \\
&\leq 5 \mathbb{E} \left[\left(\int_0^r (\|\nabla f(\mathbf{x}_{k-1} + s\mathbf{u}_k) - \nabla f(\mathbf{x}_{k-1})\| + \|\nabla f(\mathbf{x}_{k-1} + s\mathbf{u}_{k-1}) - \nabla f(\mathbf{x}_{k-1})\|) ds \right)^2 \right] \\
&\quad + \frac{5}{4} r^2 \mathbb{E} [|\langle \nabla f(\mathbf{x}_{k-1}), \mathbf{u}_k - \mathbf{u}_{k-1} \rangle|^2] \\
&\leq 5 \mathbb{E} \left[\left(\int_0^r (Ls \|\mathbf{u}_k\| + Ls \|\mathbf{u}_{k-1}\|) ds \right)^2 \right] \\
&\quad + \frac{5}{4} r^2 \mathbb{E} [\nabla f(\mathbf{x}_{k-1})^\top \mathbb{E} [(\mathbf{u}_k - \mathbf{u}_{k-1})(\mathbf{u}_k - \mathbf{u}_{k-1})^\top | \mathcal{F}_{k-1}] \nabla f(\mathbf{x}_{k-1})] \\
&= 5r^4 L^2 + \frac{5r^2}{2d} \mathbb{E} [\|\nabla f(\mathbf{x}_{k-1})\|^2]
\end{aligned}$$

where we used $\|\mathbf{u}_k\| = \|\mathbf{u}_{k-1}\| = 1$ and

$$\mathbb{E} [(\mathbf{u}_k - \mathbf{u}_{k-1})(\mathbf{u}_k - \mathbf{u}_{k-1})^\top | \mathcal{F}_{k-1}] = \frac{2}{d} I_d,$$

and for the second term, we have

$$\mathbb{E} [|f(\mathbf{x}_k + r\mathbf{u}_k) - f(\mathbf{x}_{k-1} + r\mathbf{u}_k)|^2] \leq G^2 \mathbb{E} [\|\mathbf{x}_k - \mathbf{x}_{k-1}\|^2] = G^2 \mathbb{E} [\|\mathbf{p}_{k-1}\|^2].$$

Therefore for $k > 1$,

$$\mathbb{E} [|z_k|^2] \leq (1-\tilde{\beta}) \mathbb{E} [|z_{k-1}|^2] + \frac{5r^2}{\tilde{\beta}d} \mathbb{E} [\|\nabla f(\mathbf{x}_{k-1})\|^2] + \frac{10r^4 L^2}{\tilde{\beta}} + \frac{2G^2}{\tilde{\beta}} \mathbb{E} [\|\mathbf{p}_{k-1}\|^2].$$

By summing over $k = 1, \dots, T$, we get

$$\sum_{k=1}^T \mathbb{E} [|z_k|^2] \leq (1-\tilde{\beta}) \sum_{k=1}^{T-1} \mathbb{E} [|z_{k-1}|^2] + \frac{5r^2}{\tilde{\beta}d} \sum_{k=1}^{T-1} \mathbb{E} [\|\nabla f(\mathbf{x}_{k-1})\|^2] + \frac{10(T-1)r^4 L^2}{\tilde{\beta}}$$

$$\begin{aligned}
& + \frac{2G^2}{\tilde{\beta}} \sum_{k=1}^{T-1} \mathbb{E}[\|\mathbf{p}_{k-1}\|^2] + \frac{5r^2}{4d} \mathbb{E}[\|\nabla f(\mathbf{x}_1)\|^2] + \frac{5r^4 L^2}{4} \\
& \leq (1-\tilde{\beta}) \sum_{k=1}^T \mathbb{E}[|z_{k-1}|^2] + \frac{25r^2}{4\tilde{\beta}d} \sum_{k=1}^{T-1} \mathbb{E}[\|\nabla f(\mathbf{x}_{k-1})\|^2] + \frac{10Tr^4 L^2}{\tilde{\beta}} \\
& + \frac{2G^2}{\tilde{\beta}} \sum_{k=1}^{T-1} \mathbb{E}[\|\mathbf{p}_{k-1}\|^2],
\end{aligned}$$

which then implies the desired result. \square

The following lemma then provides bounds for the accumulated second moment of \mathbf{g}_k and \mathbf{p}_k .

Lemma 3. *Suppose the quantity*

$$\theta := 1 - \frac{4\eta^2 d^2 G^2 (1 + \alpha^2)}{\tilde{\beta}^2 r^2 (1 - \alpha^2)^2}$$

is positive. Then we have

$$\sum_{k=1}^T \mathbb{E}[\|\mathbf{g}_k\|^2] \leq \frac{25d}{4\theta\tilde{\beta}^2} \sum_{k=1}^T \mathbb{E}[\|\nabla f(\mathbf{x}_k)\|^2] + \frac{10Tr^2 L^2 d^2}{\theta\tilde{\beta}^2}, \quad (22)$$

$$\sum_{k=1}^T \mathbb{E}[\|\mathbf{p}_k\|^2] \leq \frac{2\eta^2(1 + \alpha^2)}{(1 - \alpha^2)^2} \sum_{k=1}^T \mathbb{E}[\|\mathbf{g}_k\|^2]. \quad (23)$$

Proof. By the definition of \mathbf{p}_k , we have

$$\begin{aligned}
\mathbb{E}[\|\mathbf{p}_k\|^2] & \leq \left(1 + \frac{1 - \alpha^2}{2\alpha^2}\right) \alpha^2 \mathbb{E}[\|\mathbf{p}_{k-1}\|^2] + \left(1 + \frac{2\alpha^2}{1 - \alpha^2}\right) \eta^2 \mathbb{E}[\|\mathbf{g}_k\|^2] \\
& = \frac{1 + \alpha^2}{2} \mathbb{E}[\|\mathbf{p}_{k-1}\|^2] + \frac{1 + \alpha^2}{1 - \alpha^2} \eta^2 \mathbb{E}[\|\mathbf{g}_k\|^2].
\end{aligned}$$

By summing over $k = 1, \dots, T$, we get

$$\sum_{k=1}^T \mathbb{E}[\|\mathbf{p}_k\|^2] \leq \frac{1 + \alpha^2}{2} \sum_{k=1}^{T-1} \mathbb{E}[\|\mathbf{p}_{k-1}\|^2] + \frac{1 + \alpha^2}{1 - \alpha^2} \eta^2 \sum_{k=1}^T \mathbb{E}[\|\mathbf{g}_k\|^2],$$

which then implies (23).

Now, since $\mathbf{g}_k = \frac{d}{r} z_k \mathbf{u}_k$ and $\|\mathbf{u}_k\| = 1$, we see that $\mathbb{E}[\|\mathbf{g}_k\|^2] = \frac{d^2}{r^2} \mathbb{E}[|z_k|^2]$. By using the bound in Lemma 2, we get

$$\sum_{k=1}^T \mathbb{E}[\|\mathbf{g}_k\|^2] \leq \sum_{k=1}^{T-1} \frac{2d^2 G^2}{\tilde{\beta}^2 r^2} \mathbb{E}[\|\mathbf{p}_k\|^2] + \frac{25d}{4\tilde{\beta}^2} \sum_{k=1}^{T-1} \mathbb{E}[\|\nabla f(\mathbf{x}_k)\|^2] + \frac{10Tr^2 L^2 d^2}{\tilde{\beta}^2},$$

After plugging in the bound (23), we can show that

$$\left(1 - \frac{4\eta^2 d^2 G^2 (1 + \alpha^2)}{\tilde{\beta}^2 r^2 (1 - \alpha^2)^2}\right) \sum_{k=1}^T \mathbb{E}[\|\mathbf{g}_k\|^2] \leq \frac{25d}{4\tilde{\beta}^2} \sum_{k=1}^T \mathbb{E}[\|\nabla f(\mathbf{x}_k)\|^2] + \frac{10Tr^2 L^2 d^2}{\tilde{\beta}^2},$$

which gives (22). \square

B Proof of Theorem 1

Denote $\mathbf{w}_k := \mathbf{x}_k - \alpha \mathbf{p}_{k-1} / (1 - \alpha)$. We have

$$\mathbf{w}_{k+1} = \mathbf{x}_{k+1} - \frac{\alpha}{1 - \alpha} \mathbf{p}_k = \mathbf{x}_k - \frac{1}{1 - \alpha} \mathbf{p}_k = \mathbf{x}_k - \frac{\alpha}{1 - \alpha} \mathbf{p}_{k-1} - \frac{\eta}{1 - \alpha} \mathbf{g}_k = \mathbf{w}_k - \frac{\eta}{1 - \alpha} \mathbf{g}_k,$$

and so

$$\|\mathbf{w}_{k+1} - \mathbf{x}^*\|^2 = \|\mathbf{w}_k - \mathbf{x}^*\|^2 - \frac{2\eta}{1-\alpha} \langle \mathbf{w}_k - \mathbf{x}^*, \mathbf{g}_k \rangle + \frac{\eta^2}{(1-\alpha)^2} \|\mathbf{g}_k\|^2.$$

By taking the expectation conditioned on \mathcal{F}_k , we get

$$\begin{aligned} \mathbb{E}[\|\mathbf{w}_{k+1} - \mathbf{x}^*\|^2 | \mathcal{F}_k] &= \|\mathbf{w}_k - \mathbf{x}^*\|^2 - \frac{2\eta}{1-\alpha} \langle \mathbf{w}_k - \mathbf{x}^*, \nabla f_r(\mathbf{x}_k) \rangle + \frac{\eta^2}{(1-\alpha)^2} \mathbb{E}[\|\mathbf{g}_k\|^2 | \mathcal{F}_k] \\ &= \|\mathbf{w}_k - \mathbf{x}^*\|^2 - \frac{2\eta}{1-\alpha} \langle \mathbf{x}_k - \mathbf{x}^*, \nabla f_r(\mathbf{x}_k) \rangle \\ &\quad - \frac{2\eta\alpha}{(1-\alpha)^2} \langle \mathbf{x}_k - \mathbf{x}_{k-1}, \nabla f_r(\mathbf{x}_k) \rangle + \frac{\eta^2}{(1-\alpha)^2} \mathbb{E}[\|\mathbf{g}_k\|^2 | \mathcal{F}_k]. \end{aligned}$$

Noticing that the convexity of f implies

$$\begin{aligned} -\langle \mathbf{x}_k - \mathbf{x}_{k-1}, \nabla f_r(\mathbf{x}_k) \rangle &\leq -(f_r(\mathbf{x}_k) - f_r(\mathbf{x}_{k-1})), \\ -\langle \mathbf{x}_k - \mathbf{x}^*, \nabla f_r(\mathbf{x}_k) \rangle &\leq -(f_r(\mathbf{x}_k) - f_r(\mathbf{x}^*)), \end{aligned}$$

we get

$$\begin{aligned} \mathbb{E}[\|\mathbf{w}_{k+1} - \mathbf{x}^*\|^2] &\leq \mathbb{E}[\|\mathbf{w}_k - \mathbf{x}^*\|^2] - \frac{2\eta}{1-\alpha} (f_r(\mathbf{x}_k) - f_r(\mathbf{x}^*)) \\ &\quad - \frac{2\eta\alpha}{(1-\alpha)^2} (f_r(\mathbf{x}_k) - f_r(\mathbf{x}_{k-1})) + \frac{\eta^2}{(1-\alpha)^2} \mathbb{E}[\|\mathbf{g}_k\|^2]. \end{aligned}$$

Now let us assume $\theta := 1 - 4\eta^2 d^2 G^2 (1 + \alpha^2) / [\tilde{\beta}^2 r^2 (1 - \alpha^2)^2] > 0$. By taking the telescoping sum over $k = 1, \dots, T$ and plugging in the bound on $\sum_{k=1}^T \mathbb{E}[\|\mathbf{g}_k\|^2]$ in Lemma 3, we get

$$\begin{aligned} \mathbb{E}[\|\mathbf{w}_{T+1} - \mathbf{x}^*\|^2] &\leq \|\mathbf{w}_1 - \mathbf{x}^*\|^2 - \frac{2\eta}{1-\alpha} \sum_{k=1}^T \mathbb{E}[f_r(\mathbf{x}_k) - f_r(\mathbf{x}^*)] - \frac{2\eta\alpha}{(1-\alpha)^2} \mathbb{E}[f_r(\mathbf{x}_T) - f_r(\mathbf{x}_1)] \\ &\quad + \frac{25\eta^2 Ld}{2(1-\alpha)^2 \theta \tilde{\beta}^2} \sum_{k=1}^T \mathbb{E}[f(\mathbf{x}_k) - f(\mathbf{x}^*)] + \frac{10T\eta^2 r^2 L^2 d^2}{(1-\alpha)^2 \theta \tilde{\beta}^2}, \end{aligned}$$

where we also used the inequality $\|\nabla f(\mathbf{x}_k)\|^2 \leq 2L(f(\mathbf{x}_k) - f(\mathbf{x}^*))$ (see [26, Eq. (2.1.7)]). By Lemma 1, we get

$$\begin{aligned} \mathbb{E}[\|\mathbf{w}_{T+1} - \mathbf{x}^*\|^2] &\leq \|\mathbf{w}_1 - \mathbf{x}^*\|^2 - \frac{2\eta}{1-\alpha} \sum_{k=1}^T \mathbb{E}[f(\mathbf{x}_k) - f(\mathbf{x}^*)] - \frac{2\eta\alpha}{(1-\alpha)^2} \mathbb{E}[f(\mathbf{x}_T) - f(\mathbf{x}_1)] \\ &\quad + \frac{25\eta^2 Ld}{2(1-\alpha)^2 \theta \tilde{\beta}^2} \sum_{k=1}^T \mathbb{E}[f(\mathbf{x}_k) - f(\mathbf{x}^*)] + \frac{10T\eta^2 r^2 L^2 d^2}{(1-\alpha)^2 \theta \tilde{\beta}^2} + \frac{\eta T r^2 L}{1-\alpha} + \frac{\eta \alpha r^2 L}{(1-\alpha)^2}, \end{aligned}$$

which further leads to

$$\begin{aligned} &\left(1 - \frac{25\eta Ld}{4(1-\alpha)\theta \tilde{\beta}^2}\right) \frac{1}{T} \sum_{k=1}^T \mathbb{E}[f(\mathbf{x}_k) - f(\mathbf{x}^*)] + \frac{\alpha}{1-\alpha} \frac{\mathbb{E}[f(\mathbf{x}_T) - f(\mathbf{x}^*)]}{T} \\ &\leq \frac{(1-\alpha)\|\mathbf{x}_1 - \mathbf{x}^*\|^2}{2\eta T} + \frac{5\eta r^2 L^2 d^2}{(1-\alpha)\theta \tilde{\beta}^2} + \frac{r^2 L}{2} + \frac{\alpha r^2 L}{2(1-\alpha)T} + \frac{\alpha}{1-\alpha} \frac{f(\mathbf{x}_1) - f(\mathbf{x}^*)}{T}. \end{aligned}$$

Now, by letting

$$\eta \leq \frac{(1-\alpha)\tilde{\beta}^2}{25LdT^{1/3}}, \quad \frac{4\eta dG}{\tilde{\beta}(1-\alpha)} \leq r \leq \frac{G}{LT^{1/3}},$$

we see that

$$\theta \geq 1 - \frac{1}{4} \cdot \frac{(1+\alpha^2)}{(1+\alpha)^2} \geq \frac{3}{4}, \quad 1 - \frac{25\eta Ld}{4(1-\alpha)\theta \tilde{\beta}^2} \geq 1 - \frac{1}{3T^{1/3}} \geq \frac{2}{3},$$

and then we obtain

$$\frac{1}{T} \sum_{k=1}^T \mathbb{E}[f(\mathbf{x}_k) - f(\mathbf{x}^*)] \leq \frac{3(1-\alpha)\|\mathbf{x}_1 - \mathbf{x}^*\|^2}{4\eta T} + \frac{3G^2}{4LT^{2/3}} + O(d/T),$$

which implies the desired bound as f is convex.

C Proof of the Nonconvex Case

We let $\mathbf{w}_k := \mathbf{x}_k - \alpha \mathbf{p}_{k-1} / (1 - \alpha)$, and it can be checked that $\mathbf{w}_{k+1} = \mathbf{w}_k - \eta \mathbf{g}_k / (1 - \alpha)$. By the L -smoothness of f , we have

$$\begin{aligned} f(\mathbf{w}_{k+1}) &\leq f(\mathbf{w}_k) - \frac{\eta}{1-\alpha} \langle \mathbf{g}_k, \nabla f(\mathbf{z}_k) \rangle + \frac{\eta^2 L}{2(1-\alpha)^2} \|\mathbf{g}_k\|^2 \\ &= f(\mathbf{w}_k) - \frac{\eta}{1-\alpha} \langle \mathbf{g}_k, \nabla f(\mathbf{w}_k) - \nabla f(\mathbf{x}_k) \rangle - \frac{\eta}{1-\alpha} \langle \mathbf{g}_k, \nabla f(\mathbf{x}_k) \rangle + \frac{\eta^2 L}{2(1-\alpha)^2} \|\mathbf{g}_k\|^2. \end{aligned}$$

By taking the expectation conditioned on \mathcal{F}_k , we get

$$\begin{aligned} \mathbb{E}[f(\mathbf{w}_{k+1}) | \mathcal{F}_k] &\leq f(\mathbf{w}_k) - \frac{\eta}{1-\alpha} \langle \nabla f_r(\mathbf{x}_k), \nabla f(\mathbf{w}_k) - \nabla f(\mathbf{x}_k) \rangle - \frac{\eta}{1-\alpha} \langle \nabla f_r(\mathbf{x}_k), \nabla f(\mathbf{x}_k) \rangle \\ &\quad + \frac{\eta^2 L}{2(1-\alpha)^2} \mathbb{E}[\|\mathbf{g}_k\|^2 | \mathcal{F}_k]. \end{aligned}$$

Note that

$$\begin{aligned} & - \langle \nabla f_r(\mathbf{x}_k), \nabla f(\mathbf{w}_k) - \nabla f(\mathbf{x}_k) \rangle \\ &= - \langle \nabla f(\mathbf{x}_k), \nabla f(\mathbf{w}_k) - \nabla f(\mathbf{x}_k) \rangle - \langle \nabla f_r(\mathbf{x}_k) - \nabla f(\mathbf{x}_k), \nabla f(\mathbf{w}_k) - \nabla f(\mathbf{x}_k) \rangle \\ &\leq \frac{1}{4} \|\nabla f(\mathbf{x}_k)\|^2 + \|\nabla f_r(\mathbf{x}_k) - \nabla f(\mathbf{x}_k)\|^2 + \frac{5}{4} \|\nabla f(\mathbf{w}_k) - \nabla f(\mathbf{x}_k)\|^2 \\ &\leq \frac{1}{4} \|\nabla f(\mathbf{x}_k)\|^2 + L^2 r^2 + \frac{5}{4} L^2 \|\mathbf{w}_k - \mathbf{x}_k\|^2 \\ &= \frac{1}{4} \|\nabla f(\mathbf{x}_k)\|^2 + L^2 r^2 + \frac{5L^2 \alpha^2}{4(1-\alpha)^2} \|\mathbf{p}_{k-1}\|^2, \end{aligned}$$

and

$$\begin{aligned} - \langle \nabla f_r(\mathbf{x}_k), \nabla f(\mathbf{x}_k) \rangle &= - \|\nabla f(\mathbf{x}_k)\|^2 - \langle \nabla f_r(\mathbf{x}_k) - \nabla f(\mathbf{x}_k), \nabla f(\mathbf{x}_k) \rangle \\ &\leq - \frac{3}{4} \|\nabla f(\mathbf{x}_k)\|^2 + \|\nabla f_r(\mathbf{x}_k) - \nabla f(\mathbf{x}_k)\|^2 \\ &\leq - \frac{3}{4} \|\nabla f(\mathbf{x}_k)\|^2 + L^2 r^2. \end{aligned}$$

Therefore

$$\begin{aligned} \mathbb{E}[f(\mathbf{w}_{k+1}) | \mathcal{F}_k] &\leq f(\mathbf{w}_k) - \frac{\eta}{2(1-\alpha)} \|\nabla f(\mathbf{x}_k)\|^2 + \frac{2\eta r^2 L^2}{1-\alpha} \\ &\quad + \frac{5\eta L^2 \alpha^2}{4(1-\alpha)^3} \|\mathbf{p}_{k-1}\|^2 + \frac{\eta^2 L}{2(1-\alpha)^2} \mathbb{E}[\|\mathbf{g}_k\|^2 | \mathcal{F}_k]. \end{aligned}$$

Now, by taking the total expectation and summing over $k = 1, \dots, T$, we get

$$\begin{aligned} \mathbb{E}[f(\mathbf{w}_{T+1})] &\leq f(\mathbf{w}_1) - \frac{\eta}{2(1-\alpha)} \sum_{k=1}^T \mathbb{E}[\|\nabla f(\mathbf{x}_k)\|^2] + \frac{2\eta r^2 L^2 T}{1-\alpha} \\ &\quad + \frac{5\eta L^2 \alpha^2}{4(1-\alpha)^3} \sum_{k=1}^{T-1} \mathbb{E}[\|\mathbf{p}_k\|^2] + \frac{\eta^2 L}{2(1-\alpha)^2} \sum_{k=1}^T \mathbb{E}[\|\mathbf{g}_k\|^2]. \end{aligned}$$

Assuming $\theta := 1 - 4\eta^2 d^2 G^2 (1 + \alpha^2) / [\tilde{\beta}^2 r^2 (1 - \alpha^2)^2] > 0$ and plugging in the bounds in Lemma 3, we get

$$\begin{aligned} \mathbb{E}[f(\mathbf{w}_{T+1})] &\leq f(\mathbf{w}_1) - \frac{\eta}{2(1-\alpha)} \sum_{k=1}^T \mathbb{E}[\|\nabla f(\mathbf{x}_k)\|^2] + \frac{2\eta r^2 L^2 T}{1-\alpha} \\ &\quad + \frac{\eta^2 L}{2(1-\alpha)^2} \left(1 + \frac{5\eta L \alpha^2 (1 + \alpha^2)}{(1-\alpha)^3 (1 + \alpha)^2} \right) \left(\frac{25d}{4\theta \tilde{\beta}^2} \sum_{k=1}^T \mathbb{E}[\|\nabla f(\mathbf{x}_k)\|^2] + \frac{10Tr^2 L^2 d^2}{\theta \tilde{\beta}^2} \right). \end{aligned}$$

Now let T be sufficiently large such that

$$T^{1/3} \geq \frac{10\alpha^2\tilde{\beta}^2}{25d(1-\alpha)^2},$$

and let

$$\eta \leq \frac{(1-\alpha)\tilde{\beta}^2}{25LdT^{1/3}}, \quad \frac{4\eta dG}{\tilde{\beta}(1-\alpha)} \leq r \leq \frac{G}{LT^{1/3}},$$

We then have $\eta \leq (1-\alpha)^3/(10\alpha^2L)$, and so

$$\theta \geq 1 - \frac{1}{4} \cdot \frac{(1+\alpha^2)}{(1+\alpha)^2} \geq \frac{3}{4}, \quad \frac{5\eta L\alpha^2(1+\alpha^2)}{(1-\alpha)^3(1+\alpha)^2} \leq \frac{1+\alpha^2}{2(1+\alpha)^2} \leq \frac{1}{2}.$$

Therefore

$$\begin{aligned} \mathbb{E}[f(\mathbf{w}_{T+1})] &\leq f(\mathbf{w}_1) - \frac{\eta}{2(1-\alpha)} \left(1 - \frac{25\eta Ld}{2(1-\alpha)\tilde{\beta}^2}\right) \sum_{k=1}^T \mathbb{E}[\|\nabla f(\mathbf{x}_k)\|^2] \\ &\quad + \frac{2\eta r^2 L^2 T}{1-\alpha} + \frac{\eta^2 L}{(1-\alpha)^2 \tilde{\beta}^2} \cdot 10Tr^2 L^2 d^2 \\ &\leq f(\mathbf{x}_1) - \frac{\eta}{4(1-\alpha)} \sum_{k=1}^T \mathbb{E}[\|\nabla f(\mathbf{x}_k)\|^2] + \frac{\eta}{1-\alpha} \cdot 2G^2 T^{1/3} + \frac{\eta}{1-\alpha} \cdot \frac{2G^2 d}{5}, \end{aligned}$$

which leads to

$$\frac{1}{T} \sum_{k=1}^T \mathbb{E}[\|\nabla f(\mathbf{x}_k)\|^2] \leq \frac{4(1-\alpha)(f(\mathbf{x}_1) - f^*)}{\eta T} + \frac{8G^2}{T^{2/3}} + \frac{8G^2 d}{5T}.$$